Dyes and Pigments 87 (2010) 125–131

Contents lists available at ScienceDirect

Dyes and Pigments

journal homepage: www.elsevier.com/locate/dyepig

The environmentally benign synthesis of nanosized $Co_xZn_{1-x}Al_2O_4$ blue pigments

Diana Visinescu [a,*], Carmen Paraschiv [b], Adelina Ianculescu [c], Bogdan Jurca [d], Bogdan Vasile [c], Oana Carp [a,*]

[a] Romanian Academy, Institute of Physical Chemistry "Ilie Murgulescu", Coordination and Supramolecular Chemistry Laboratory, Splaiul Independenței 202, 060021 Bucharest, Romania
[b] National Institute for Research and Development in Electrical Engineering, ICPE-CA, Advanced Research, Splaiul Unirii 313, 030138 Bucharest, Romania
[c] University Politehnica of Bucharest, Gh. Polizu Street no.1-7, 011061 Bucharest, Romania
[d] University of Bucharest, Physical Chemistry Department, Bd. Elisabeta 4-12, 030018 Bucharest, Romania

ARTICLE INFO

Article history:
Received 24 August 2009
Received in revised form
1 March 2010
Accepted 5 March 2010
Available online 15 March 2010

Keywords:
Environmentally friendly synthesis
Starch
Spinel
Cobalt zinc aluminate
Blue pigment

ABSTRACT

Nanosized $Co_xZn_{1-x}Al_2O_4$ ($x = 0$, 0.1, 0.2, 0.4, 0.6, 0.8 and 1) blue pigments were prepared using a novel, starch-based synthetic route, in which the carbohydrate acts as chelating, template and gelation agent. The (Zn,Al,Co)-starch gel precursors were characterized using FTIR and thermal analysis, while their corresponding oxides were characterized using FTIR, NIR-UV–Vis spectroscopy, XRD and SEM. The FTIR spectra of the pink-reddish metals-starch gel precursors, dried at 80 °C, indicated the formation of a complex (Zn,Al,Co)-starch assembly as well as the first signs of a spinelic phase. Thermal analysis of the precursors showed that mass loss was accomplished at ~ 430 °C; for $Co_xZn_{1-x}Al_2O_4$ ($0 \leq x \leq 0.6$) metal-oxide samples the spinel crystallization phase transformation occurred in the temperature range ~700–830 °C. The presence of a pure spinel lattice after calcination of the metal-starch gel precursors at 800 °C was confirmed; particles were homogeneous in shape and size, with a pronounced tendency to form agglomerates and aggregatess. NIR-UV–Vis spectra of the blue oxides were characteristic of Co(II) metal ions located in tetrahedral sites and also showed disorder dependence on cobalt(II) cation-content.

1. Introduction

Thernard's Blue namely, cobalt (II) aluminate spinel, $CoAl_2O_4$, is one of the most popular of inorganic pigments [1] and its physico-chemical features, such as high thermal and chemical stability, high resistance to acids, alkalis, light and various atmospheric agents make it suitable for various industrial applications, such as ceramics, glass, plastics, paint, paper, rubber, and color TV tubes [2–6].

As many blue inorganic pigments [1], the key elements for cobalt (II)-based aluminate oxides are the constituent Co(II) cations, which are usually located on tetrahedral sites within a conventional, cubic, spinel-type structure and are the source of the observed blue color. However, the preparation of blue aluminate pigments suffers several disadvantages that arise from the fact that cobalt is scarce, expensive and, most importantly, toxic (cobalt is included in the European Council Decision 94/904/EC and Council Directive 91/689/EEC). In this context, the reduction of the cobalt content of such oxide pigments would prove of value, from an environmental perspective, assuming that its coloration properties could be maintained.

It is well-known that the method of synthesis is crucial in terms of oxide-based pigment characteristics and that the synthetic method used can be adapted to achieve the desired properties. Conventional high-temperature solid-state reactions between two oxide components were used to prepare ceramic oxide-based pigments with superior hiding properties [7–10]. Various *chimie douce* (soft chemistry) techniques namely sol-gel and polyol methods, hydrothermal synthesis as well as thermal decomposition of metal-organic precursors have offered wide possibilities in the synthesis of high purity, homogeneous, nanosized aluminate particles of narrow size distribution, which result in improved optical and coating properties [6,11–22]. Recently, a polymeric precursor method involving citric acid and ethylene-glycol was used to obtain cobalt(II)-aluminates containing a reduced amount of cobalt [23]. Although low temperature synthesis of $CoAl_2O_4$ oxide aluminates (temperatures starting from 450 °C) have been reported,

* Corresponding authors. Tel.: +40 21367912; fax: +40 213121147.
E-mail addresses: diana.visinescu@gmail.com (D. Visinescu), carp@acodarom.ro (O. Carp).

0143-7208/$ – see front matter © 2010 Elsevier Ltd. All rights reserved.
doi:10.1016/j.dyepig.2010.03.006

no information about their coloration properties has been provided [12,22]. A common temperature for the synthesis of the blue-colored $CoAl_2O_4$ pigment is >800 °C [16].

Less attention has been paid, unfortunately, to more environmentally aware synthesis of oxide-based pigments. Usually, a non-polluting method is associated with non-toxic raw materials and reaction intermediates as well as minimal energy usage. This paper concerns a novel, less-toxic, flexible and reproducible starch-based synthesis of cobalt aluminate oxide spinels, $Co_xZn_{1-x}Al_2O_4$ ($x = 0$, 0.1, 0.2, 0.4, 0.6, 0.8 and 1), which comprise the gradual insertion of Co(II) cations within a gahnite ($ZnAl_2O_4$) host lattice. The carbohydrate has a triple role during the synthesis as complexing, template and gelation agent.

The soluble starch is a low-cost, abundant, renewable, natural polysaccharide and thus fulfils environmentally aware chemistry demands. The starch has already been employed as a powerful tool for controlling the particle shape and size of inorganic materials [24–33] and carries a large number of functional polyol groups, thereby acting as a ligand towards divalent or trivalent metal ions. Moreover, at ~80–90 °C, the resulting complex precursors, in the presence of an excess of starch, form gels. The host zinc aluminate lattice was not chosen randomly but, rather, because $ZnAl_2O_4$ is non-toxic/non-hazardous. The toxicities of ZnO and Al_2O_3 are low ($\mathbf{LD_{50}}$ = 5000 mg kg^{-1} for ZnO and 15 000 mg/kg for Al_2O_3). Furthermore, both zinc and aluminum metals are abundant in the earth's crust and $ZnAl_2O_4$ displays high thermal and chemical stability. The versatility of the spinelic structure regarding cation distribution is also noteworthy, as the tetrahedral/octahedral occupied sites ratio for a cation is dictated mainly by the oxide's thermal history.

2. Experimental

The chemicals were purchased from commercial sources: cobalt acetate [$Co(CH_3COO)_2{\cdot}4H_2O$, Reactivul], zinc acetate [$Zn(CH_3COO)_2{\cdot}2H_2O$, Reactivul], aluminum nitrate [$Al(NO_3)_3{\cdot}9H_2O$, Merck] and starch [$(C_6H_{10}O_5)_n$, Carl Roth]. All manipulations were performed using materials as received.

2.1. Synthesis

2.1.1. Metals-starch gel precursors

An aqueous solution containing Zn(II), Al(III) and Co(II) metal ion salts and starch was heated at 60 °C, under continuous stirring. After 1 h, the temperature was raised to 80 °C and the mixture was stirred for several hours until a pink-reddish gel was formed. The used ratio M(II)/Al(III) [M(II) = Zn and Co] is 0.5 and M_{total}/starch [M_{total} = M(II) and Al(III)] was 2.4.

2.1.2. $Co_xZn_{1-x}Al_2O_4$ ($x = 0.1, 0.2, 0.4, 0.6, 0.8, 1$) oxides

The blue mixed oxide have been obtained after a heat treatment of the metal-starch gels precursors at T = 800 °C, for 1 h, with a heating rate of 20 K/min.

2.2. Thermal investigations

The thermal analysis have been carried out under static air, with sample mass about ~10 mg at heating rates of 5 K/min on a Netzch thermo balance STA 409 PC/PG type.

2.3. Spectral investigations

The IR spectra (KBr pellets) were recorded in the 4000–400 cm^{-1} region with an FTIR Brucker Tensor V-37 spectrophotometer. UV–Vis spectra (diffuse reflectance technique) were recorded on the 200–1800 nm domain with a JASCO V-670 spectrophotometer, using MgO as a standard.

2.4. Structure and morphology

The structure of the as-resulted powders was examined at room temperature with an SHIMADZU XRD 6000 diffractometer, using Ni-filtered CuKα radiation (λ = 1.5418 Å), with a scan step of 0.02° and a counting time of 1 s/step, for 2θ ranged between (20–70)°.

In order to analyze the oxides powders morphology, crystallinity degree and to check their chemical composition and purity, TEM and HRTEM coupled with SAED (surface area electron diffraction) and EDX (energy dispersive X-ray spectroscopy) investigations were performed using a high resolution transmission electron TECNAI F30 S-Twin microscope.

3. Results and discussion

3.1. Synthesis and characterization of the metal-starch complex precursors

3.1.1. Synthesis

The combined coordinating and structure-directed effects of the starch have allowed us to easily obtain a stable (Zn, Al, Co)-starch complex which has been encapsulated within the polysaccharide (in excess) matrix (Scheme 1). Several steps of the synthesis deserve to be discussed: (i) the polysaccharide acts initially as ligand toward the metal cations and determines the formation of the metals-starch complex; (ii) the residual starch gradually coats (through a complex hydrogen-bonds supramolecular interactions) the metals-starch complexes, which, thus, will be protected against further chemical reactions. The helical form of the carbohydrate

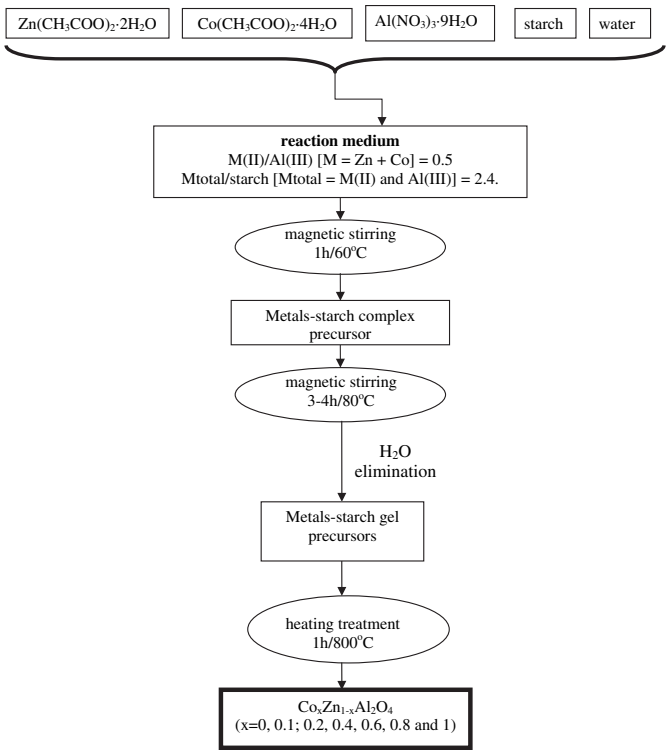

Scheme 1. The resumed synthetic pathway of the nanosized $Co_xZn_{1-x}Al_2O_4$ (x = 0, 0.1, 0.2, 0.4, 0.6, 0.8 and 1) mixed oxides.

plays a structure-director role on the supramolecular assembly; (iii) a further heating treatment, at $T \approx 80$–90 °C for several hours, is accompanied by the water elimination, the mixture being finally gelified, with the metals-starch complex "frozen" into a solid rigid network. The formation of the amorphous gel is essential to assure a high homogeneity and a good stoichiometry of the components. The preservation of a uniform distribution of cations during the thermal decompositions assures a supplementary protection against the nanoparticles segregation. As a consequence, the atomic diffusion processes are considerably reduced and the pure spinelic phase could be achieved in shorter times at lower temperatures than in solid-state reactions and even in analogue solution synthetic methods. The synthetic pathway is presented in Scheme 1.

3.1.2. FTIR spectra

The FTIR spectra of the (Zn,Al,Co)-starch gel precursors are very similar and essentially contain absorption bands from the polysaccharidic ligand. Fig. 1 exhibits the IR spectrum for gel precursor sample of $Co_{0.4}Zn_{0.6}Al_2O_4$ oxide. The stretching vibrations assigned to the C–O and of the adjacent C–C bonds overlap the 1000–1150 cm^{-1} region. A striking feature of the vibration spectra is the occurrence of a broad and strong band on the 1450–1300 cm^{-1} region, which most probably results from a multiple overlapped absorptions originated from a combination of δ(OCH), δ(COH) and δ(CCH) deformation bands and the typical nitrate band. A supplementary absorption of the NO_3^- anions embedded in the polysaccharide matrix was identified as a weak and sharp band at 833 cm^{-1}. Water gives a medium intensity band at 1632 cm^{-1} (H–O–H bending mode) and also is responsible for the broad absorption in the 3000–3500 cm^{-1} region [34]. The broadness of bands suggests rather an overlap of multiple absorptions and sustains the formation of a complicate assembly made-up from (Zn, Al, Co)-starch complexes and unreacted carbohydrate. The gels have been dried at 80 °C/1 h and it is interesting to notice, after the mild heating treatment, the formation of a spinelic phase: a low-intensity and structured absorption in the 500–700 cm^{-1} region, in which the triplet characteristics for M–O and M–O–M′ bonds of the aluminate spinels is distinguished [35–38].

3.1.3. Thermal analysis

The thermal decompositions (complex, multi-step ones, in which several processes are partial or total overlapped) show similar characteristics for all metals-starch gel precursor samples. Fig. 2 shows the TG, DTG and DTA curves recorded for a middle substitution ($x = 0.4$).

The thermal decomposition of the precursors starts with an endothermic decomposition (~50–100 °C), which could be attributed to the water evolving. The second decomposition stage (up to ~250 °C) is characterized by a first endothermic step, followed by two exothermic processes. The endothermic effect is identified as the start of the degradation process of the nitrate anions (originated from aluminum nitrate [39]) which, as the temperature is rising, it will be overlapped by the starch and acetate (resulted from zinc acetate [40]) decompositions. The change of the thermal effect from endothermic to an exothermic one is determined by the redox reaction between the evolved gaseous products with both oxidant and reducing character. The last decomposition step corresponds to the degradation process of the starch and nitrate residua. The presence of nitrate anions in the reaction intermediates until the end of the decomposition process was confirmed by FTIR spectroscopy.

Higher cobalt content is associated with lower decomposition temperatures, in the final step: a variation of the substitution parameter x from 0 to 1 determines the decrease of the $T_{max\ DTA}$ of the last exothermic decomposition process and of the final decomposition temperature from 361.2 to 347.6 °C and from 426.5 to 367.5 °C, respectively.

An exothermic phase transition, assigned to the spinel crystallization, was detected only for $Co_xZn_{1-x}Al_2O_4$ aluminates samples, in which $0 \leq x \leq 0.6$ (Fig. 3). The cobalt content increase is accompanied by the decrease of the DTA signal intensity, while the $T_{max\ DTA}$ is shifted toward lower temperatures: from ~713 °C ($x = 0$) to 684 °C ($x = 0.6$). Such a behavior may be explained by a better homogeneity of the rich-cobalt oxide samples: the phase

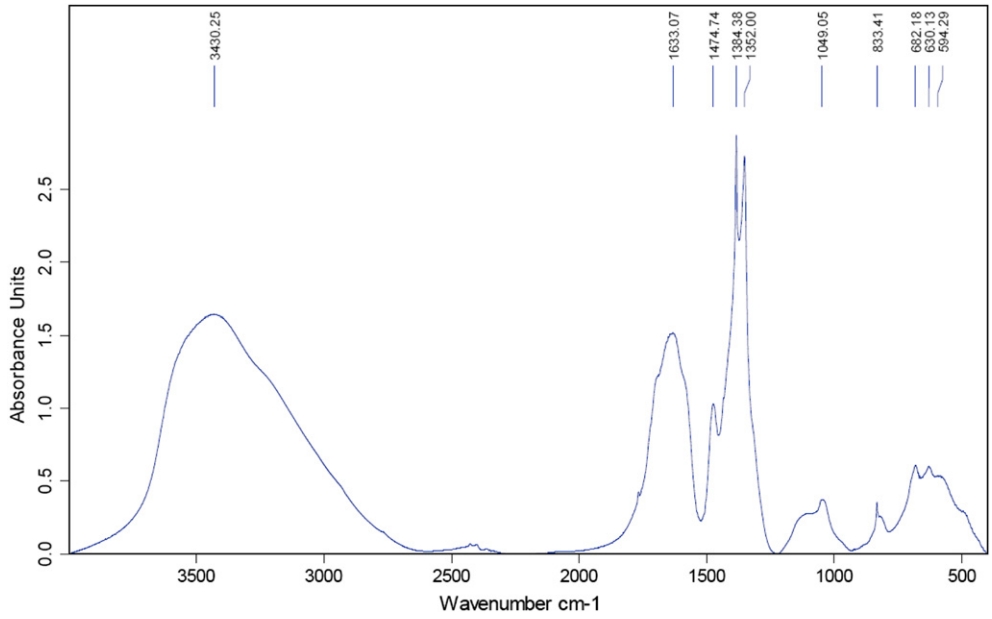

Fig. 1. FTIR spectrum for metals-starch gel precursor of $Co_{0.4}Zn_{0.6}Al_2O_4$ oxide aluminate.

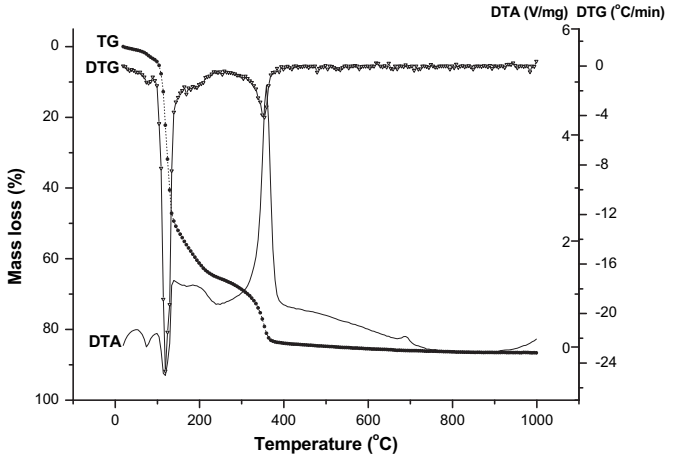

Fig. 2. Thermal curves (TG, DTG and DTA) for the metals-starch complex precursor of $Co_{0.4}Zn_{0.6}Al_2O_4$ oxide.

transition occurs more rapidly, at lower temperatures, with a lesser need of atomic diffusion.

3.2. Synthesis and characterization of Co(II)-substituted aluminates oxides

3.2.1. X-ray diffraction

Fig. 4 shows the XRD patterns of the $Co_xZn_{1-x}Al_2O_4$ ($x = 0$, 0.1, 0.2, 0.4, 0.6, 0.8 and 1) oxides samples, heated at 800 °C, for 1 h. After the calcination treatment only the diffraction peaks specific to the spinel phase were present, no secondary phases being identified.

$CoAl_2O_4$ and Co_3O_4 have very similar diffraction patterns because of their same spinel cubic structure (*Fd3m*), differing only slightly in the parameter lattice. The relative intensity of the two diffraction reflection [222]/[311] together with the presence of the [331] Bragg reflection, are considered to be the signatures of $CoAl_2O_4$ phase [41–43]. The existence of a pure $CoAl_2O_4$ ($x = 1$) phase is sustained by the I[220]/I[311] and I[331]/I[311] ratios, of 0.7 and 0.04, respectively. These values are very close to those of $CoAl_2O_4$ (0.7 and 0.04, JCPDS-82-2252), and different from the values recorded for Co_3O_4 (0.309 and 0.003, JCPDS-80-1545).

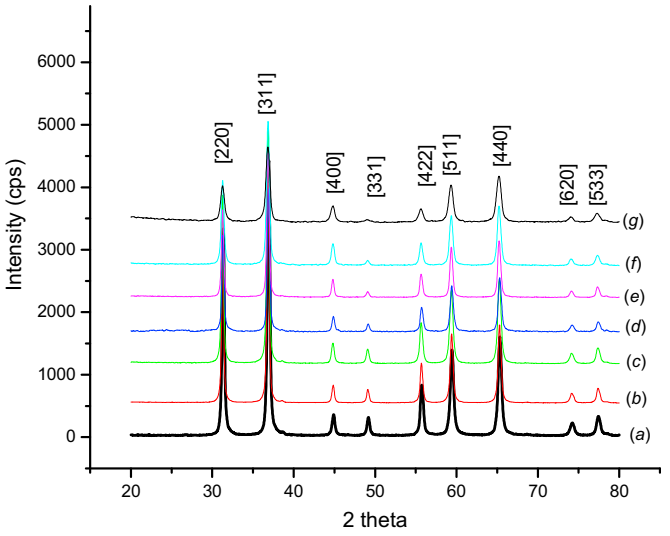

Fig. 4. Powder X-ray diffraction patterns of $Co_xZn_{1-x}Al_2O_4$ oxides [$x = 0$ (a), 0.1 (b), 0.2 (c), 0.4 (d), 0.6 (e), 0.8 (f) and 1 (g)] calcinated for 1 h at 800 °C.

The cobalt content influences the mean crystallite sizes values of the formed spinel oxides: from $ZnAl_2O_4$ ($x = 0$) to $CoAl_2O_4$ ($x = 1$) the mean crystallite sizes values continuously decreases, from 250 Å to 146 Å (heating treatment at $T = 800$ °C, for 1 h), as it is plotted in Fig. 5. An abrupt decrease has been recorded for $0.6 \leq x \leq 0.8$. These values are lower comparative with those of $Co_xZn_{1-x}Al_2O_4$ nano-oxides obtained by Pechini method (381–220 Å), after the same annealing treatment (800 °C/1 h) [23]. The reduced crystallite sizes together with the formation of spinelic phase at relatively low temperatures are two strong arguments for the efficiency and utility of the proposed synthetic route to prepare nanosized oxide-based pigments with a reduced amount of Co(II).

3.2.2. TEM, HRTEM and SAED analysis

TEM investigations indicate the formation of small particles, homogeneous as shape and size and with a pronounced tendency to form agglomerates and even aggregates. The particle average size estimated from the TEM image of $Co_{0.4}Zn_{0.6}Al_2O_4$ is ~27 nm, very close to the crystallite average size calculated from the X-ray

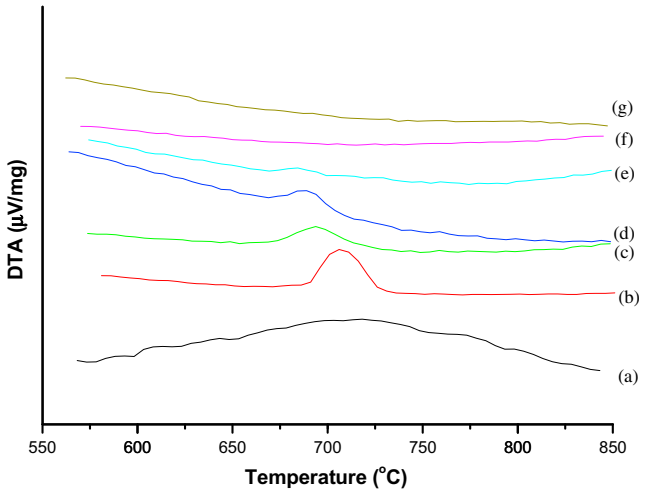

Fig. 3. DTA curves of the $Co_xZn_{1-x}Al_2O_4$ precursors [$x = 0$ (a), 0.1 (b), 0.2 (c), 0.4 (d), 0.6 (e), 0.8 (f) and 1 (g)].

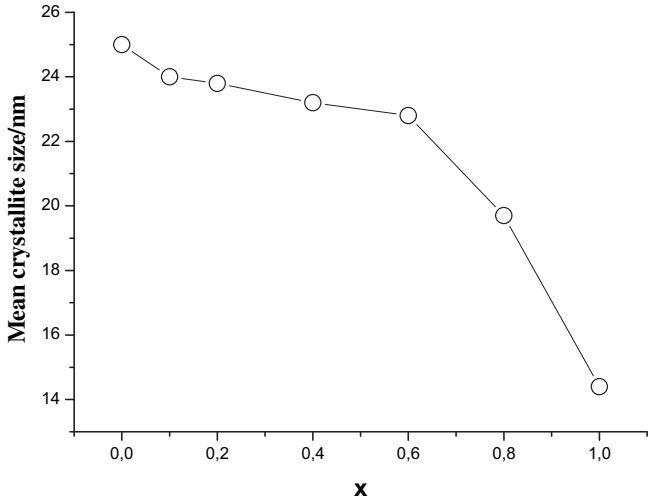

Fig. 5. Diagram of the mean crystallite size of $Co_xZn_{1-x}Al_2O_4$ oxides (calcinated for 1 h at 800 °C) vs. the cobalt (x) content.

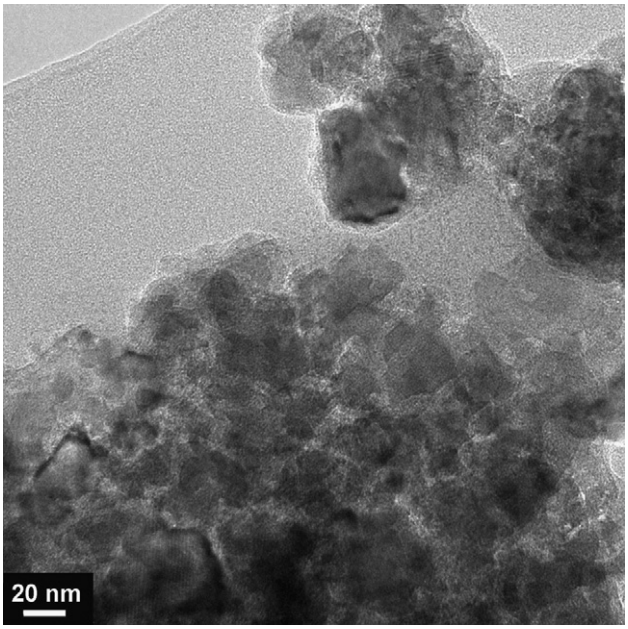

Fig. 6. TEM image of $Zn_{0.6}Co_{0.4}Al_2O_4$ powder.

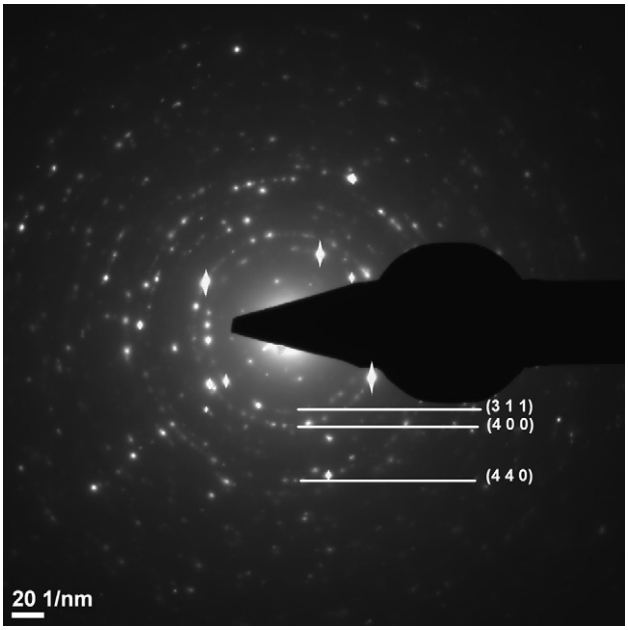

Fig. 8. SAED patterns of $Zn_{0.6}Co_{0.4}Al_2O_4$ powder.

diffraction data, proving the single crystal nature of these particles (Fig. 6). In spite of this small size, the HRTEM image from Fig. 7 clearly shows ordered fringes corresponding to the crystalline (311) planes of the spinel structure. Moreover, the SAED pattern presented in Fig. 8 also pointed out a relative high crystallinity degree. Qualitative and quantitative EDX analyses showed a high purity and suitable stoichiometry of the investigated powder.

3.2.3. Spectral properties

3.2.3.1. FTIR spectroscopy. The spinelic phase in $Co_xZn_{1-x}Al_2O_4$ ($x = 0.1, 0.2, 0.4, 0.6, 0.8, 1$) oxides is easily identified in vibration spectra as a very intense triplet in the 500–800 cm^{-1} region, specific to the M–O and M–O–M′ stretching vibrations [35–38]. Some authors associate the increase of cobalt content with a higher intensity for the absorption at ca. 650 cm^{-1}, assigned to the $[ZnO_4]$ group vibrations [23]. The analysis of the FTIR spectra of our aluminate samples reveals that no visible change of the triplet intensity occurs with the modification of the cobalt content.

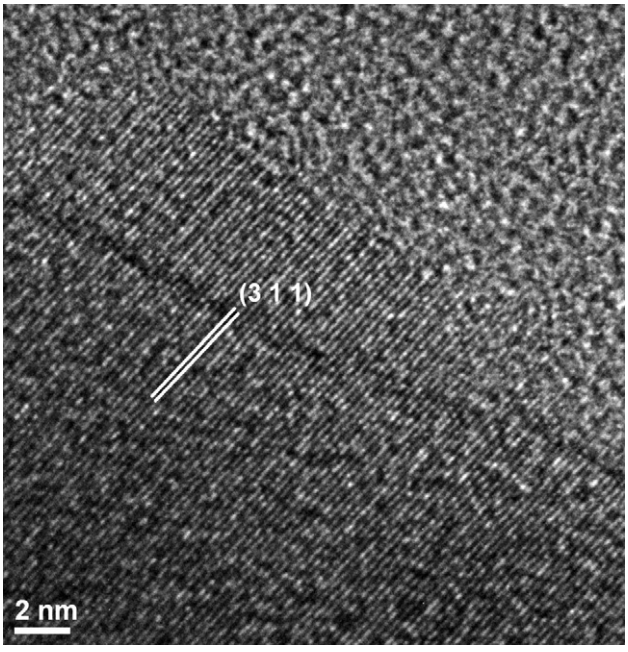

Fig. 7. HRTEM image of $Zn_{0.6}Co_{0.4}Al_2O_4$ powder.

3.2.3.2. NIR-UV–Vis spectroscopy. The color and coloring properties are fundamental characteristics of any pigment. Usually, in 3d metal cation-based pigments, their color originates mainly from the d–d allowed and/or forbidden electronic transitions. Not only the metal ion geometry, but the cristalinity degree of the samples or the crystallite sizes should be taken into account in evaluating the pigments color. Fig. 9 exhibits the visible and near infra-red diffuse reflectance spectra recorded for $Co_xZn_{1-x}Al_2O_4$ ($x = 0.1, 0.2, 0.4, 0.6, 0.8, 1$) oxides obtained at a calcination temperature of $T = 800$ °C.

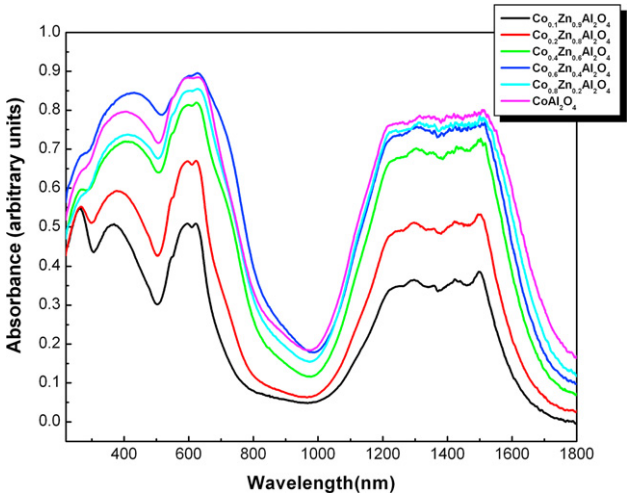

Fig. 9. Visible and near-infrared spectra for $Co_xZn_{1-x}Al_2O_4$ ($x = 0.1, 0.2, 0.4, 0.6, 0.8, 1$) oxides.

The metal-oxide samples spectra show similar features: in the visible region, a three-structured band, with maxima at ca. 544, 595 and 622 nm that gives the blue coloration of the samples. This absorption could be easily assigned to the $^4A_2(F) \rightarrow {}^4T_1(P)$ [44] spin allowed transition for the tetrahedral Co(II) chromophores. Its structured pattern is resulted most probably from the significant effects of the spin-orbit coupling which split the ^4T state in three spinor components [45,46]. A slightly blue shift of absorption is noted for the enriched-Co(II) samples, but it is still uncertain if could be related with the decrease of the mean crystallite sizes.

It is well-known that the blue-colored materials absorb visible light in the 500–700 nm and the green coloration gives a shoulder at ca. 400 nm in UV–Vis spectra. The greenish hues of our samples are associated with the large shoulder, with a maximum at ca. 360 nm. Since it is unanimously accepted that the octahedral Co^{III} cations (in Co_3O_4 oxide) are usually stable only between 400 and 700 °C [42,43,47] and the XRD and EDX investigations of our oxide samples show the presence of a pure spinelic phase, we could conclude that these absorptions mainly result from the forbidden spin transitions of the tetrahedral Co(II) cations. The absence of any absorption in the 650–800 nm region, specific for $O^{2-} \rightarrow Co^{3+}$ ligand-metal charge transfer (LMCT) is an additional argument that Co_3O_4 is not present in our oxide-systems [48]. The signature for the tetrahedral cobalt(II) metal ion is also distinguished in the NIR-region: a broad absorption with a maximum at about 1320 nm, assigned to $^4A_2 \rightarrow {}^4T_1(F)$ transition. The two shoulders located at ca. 1220 and 1500 nm are the result of the decreased tetrahedral symmetry [$^4T_1(F)$ level is split into $^4A_2 + {}^4B_1 + {}^4B_2$ levels and three bands are expected] [44].

In spinel-type oxides, the process of cation inversion is a very common phenomenon, being possible any distribution between a normal and an inverse spinel: $(A_{1-y}B_y)[B_{2-y}A_y]O_4$ (A = divalent cations, B = trivalent cations, y = inversion parameter representing the fraction of A cations in octahedral sites). The evolution of the substitution process of Zn(II) cations with Co(II) metal ions within the gahnite lattice could be easily monitored by analyzing the NIR-UV–Vis spectra. The increase in Co(II) cations concentration is accompanied by the gradual disappearance of the high energy absorptions from 260 nm (assigned to the fundamental band-to-band electron excitations in $ZnAl_2O_4$ phase) and by the enlargements of UV–Vis bands [as the result of the overlap of the allowed and forbidden spin transitions from the tetrahedral and octahedral Co(II) chromophores]. Thus, the rich-Co(II) oxides are characterized by the highest degree of spinel disorder, a percent of the Co(II) cations adopting in fact an octahedral stereochemistry.

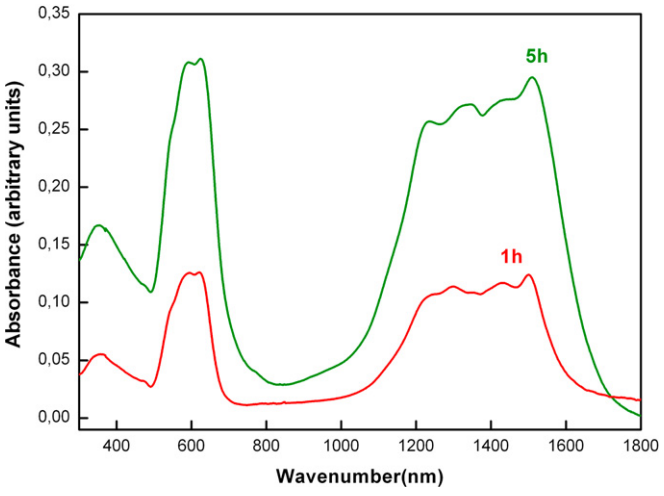

Fig. 10. Visible and NIR spectra of the poor-Co oxides, $Co_{0.1}Zn_{0.9}Al_2O_4$, obtained at 1000 °C for 1 h (red continuous line) and for 5 h (green continuous line). (For interpretation of the references to colour in figure legends, the reader is refered to the web version of this article).

The NIR-region absorptions are also affected by the Co(II) metal ions concentrations and also by the spinel inversion, the structured pattern of tetrahedral Co(II) metal ions, covering 1200–1600 nm domain, being gradually overlapped by a single broad band originating from $^4T_{1g} \rightarrow {}^4T_{2g}$ transition for octahedral Co(II) chromophores [44].

The time exposure to the heat treatment of the samples should also be considered for the pigments preparation. As shown in Fig. 10, more intense absorptions are recorded for a longtime calcined $Co_{0.1}Zn_{0.9}Al_2O_4$ oxide, effect that may attributed to the increase of the crystallites size. Further studies are currently in progress in order to clarify the influence of the calcinations temperature and time exposure to the heat treatment over the pigment quality.

4. Conclusions

The environmentally aware stages of the proposed route comprise the synthesis of a blue pigment with low cobalt content, via the use of starch in precursor build-up and the use of low temperatures that are required for spinelic phase crystallization. The precursor synthetic method involves three essential steps namely the initial formation of complexes between the metal cations and starch, followed by their encapsulation in the unreacted starch matrix, and, thence, starch gelation. Gel formation assures superior homogeneity of the precursors, which lowers the temperature required for spinel crystallization. Further heat treatment (800 °C/1 h) of the metal-starch, gel precursors leads to the desired pure, stoichiometric, high crystalline spinelic phase of the mixed-oxides, as shown by FTIR, XRD, TEM, HRTEM and SAED investigations. The mean crystallite size of the aluminate pigment samples was smaller than that of similar aluminate oxides prepared using other solution methods and depended on cobalt content, ranging from 250 Å for $ZnAl_2O_4$ ($x = 0$) to 146 Å for $CoAl_2O_4$ ($x = 1$). The optical properties of the $Co_xZn_{1-x}Al_2O_4$ (x = 0.1, 0.2, 0.4, 0.6, 0.8, 1) oxides indicate the predominant tetrahedral coordination of Co(II) cations, but also reveal a higher inversion degree for the rich-Co(II) aluminate samples.

The proposed synthetic procedure is simple, versatile and its environmental-friendly ingredients turn it into an interesting non-polluting alternative to the traditional synthesis of the oxide-based nanosized pigments.

Acknowledgements

This work was financially supported by the Romanian MECI-CNMP (PNII-Parteneriate-Project No. 32-146/2009).

References

[1] Mason RK. Use of cobalt colors in glazes. The Bulletin of American Ceramic Society 1961;40:5–6.
[2] Minuno G. In: Libri B, editor. La Fabrica dei Colori; 1995. Roma.
[3] Bauxaum G. Industrial inorganic pigments. Weinheim, Germany: VCH; 1993. p. 85.
[4] Li W, Li J, Guo J. Synthesis and characterization of nanocrystalline $CoAl_2O_4$ spinel powder by low temperature combustion. Journal of the European Ceramic Society 2003;23:2289–95.
[5] Thormählen P, Fridell E, Cruise N, Skoglundh M, Palmqvist A. The influence of CO_2, C_3H_6, NO, H_2, H_2O or SO_2 on the low-temperature oxidation of CO on a cobalt-aluminate spinel catalyst ($Co_{1.66}Al_{1.34}O_4$). Applied Catalysis B; Environmental 2001;31:1–12.

[6] Melo DMA, Cunha JD, Fernandes JDG, Bernardi MI, Melo MAF, Martinelli AE. Evaluation of $CoAl_2O_4$ as ceramic pigments. Material Research Bulletin 2003;38:1559–64.
[7] Bondioli F, Ferrari AM, Leonelli C, Manfredini T. Fabrication and characterization of ordered macroporous semiconductors CdS by colloidal crystal template. Material Research Bulletin 1998;33:723–9.
[8] Fernández Colinas JM, Otero Areán C. Kinetics of solid-state spinel formation: effect of cation coordination preference. Journal of Solid State Chemistry 1994;109:43–6.
[9] Bolt PH, Habraken FHPM, Geust JW. Formation of nickel, cobalt, copper, and iron aluminates from α- and γ-alumina-supported oxides: a comparative study. Journal of Solid State Chemistry 1998;135:59–69.
[10] Chemlal S, Larbot A, Persin M, Sarrazin J, Sghyar M, Rafiq M. Cobalt spinel $CoAl_2O_4$ via sol-gel process: elaboration and surface properties. Material Research Bulletin 2000;35:2515–23.
[11] Tseng TY, Lin JC. Preparation of fine-grained Ni-Zn ferrites. Journal of Material Science Letters 1989;8:261–2.
[12] Otero Areán C, Peñarroya Mentruit M, Escalone Platero E, Llabrés i Xamena FX. Sol–gel method for preparing high surface area $CoAl_2O_4$ and Al_2O_3–$CoAl_2O_4$ spinels. Materials Letters 1999;39:22–7.
[13] Feldmann C, Jungk H-O. Polyol-mediated preparation of nanoscale oxide particles. Angewandte Chemie International Edition 2001;40:359–62.
[14] Feldmann C. Preparation of nanoscale pigment particles. Advanced Materials 2001;13(17):1301–3.
[15] Kurihara LK, Suib SL. Sol-gel synthesis of ternary metal oxides. 1. Synthesis and characterization of MAl_2O_4 (M = Mg, Ni, Co, Cu, Fe, Zn, Mn, Cd, Ca, Hg, Sr, and Ba) and lead aluminum oxide ($Pb_2Al_2O_5$). Chemistry of Materials 1993;5:609–13.
[16] Meyer F, Hempelmann R, Mathur S, Veith M. Microemulsion mediated sol-gel synthesis of nano-scaled MAl_2O_4 (M = Co, Ni, Cu) spinels from single-source heterobimetallic alkoxide precursors. Journal of Materials Chemistry 1999;9:1755–63.
[17] Rabeneau A. The role of hydrothermal synthesis in preparative chemistry. Angewandte Chemie International Edition 1985;24:1026–40.
[18] Dawson WJ. Hydrothermal synthesis of advanced ceramic powders. American Ceramic Society Bulletin 1988;67(10):1673–7.
[19] Kutty TRN, Balachandran R. Direct precipitation of lead zirconate titanate by the hydrothermal method. Material Research Bulletin 1984;19(11): 1479–88.
[20] Lencka MM, Riman RE. Thermodynamic modeling of hydrothermal synthesis of ceramic powders. Chemistry of Materials 1993;5:61–70.
[21] Chen Z, Shi E, Li W, Zheng Y, Zhong W. Hydrothermal synthesis and optical property of nano-sized $CoAl_2O_4$ pigment. Materials Letters 2002;55:281–4.
[22] Cho WS, Kakihana M. Crystallization of ceramic pigment $CoAl_2O_4$ nanocrystals from Co–Al metal organic precursor. Journal of Alloys and Compounds 1999;287:87–90.
[23] De Souza LKC, Zamian JR, Da Rocha Filho GN, Soledade LEB, Dos Santos IMG, Souza AG, et al. Blue pigments based on $Co_xZn_{1-x}Al_2O_4$ spinels synthesized by the polymeric precursor method. Dyes and Pigments 2009;81:187–92.
[24] Veiga V, Ryan DH, Sourty E, Llanes F, Marchessault RH. Formation and characterization of superparamagnetic cross-linked high amylase starch. Carbohydrate Polymers 2000;42:353–7.
[25] Kim DK, Mikhaylova M, Wang FH, Kehr J, Bjelke B, Zhang Y, et al. Starch-coated superparamagnetic nanoparticles as MR contrast agents. Chemistry of Materials 2003;15:4343–51.
[26] Iwasaki M, Davis SA, Mann S. Spongelike macroporous TiO_2 monoliths prepared from starch gel template. Journal of Science and Technology 2004;32:99–105.
[27] Chen Y, Cao J, Zheng M, Ke X, Ji H, Liu J, et al. Novel synthesis of nanoporous nickel oxide and nickel nanoparticles/amorphous carbon composites using soluble starch as the template. Chemistry Letters 2006;35(7):700–1.
[28] Mu J, Gu Z, Sun H, Wei Q. Low temperature synthesis of Mn_3O_4 nanoparticles using starch as capping agent. Journal of Dispersion Science and Technology 2006;27:307–9.
[29] Cui X, Antonietti M, Yu S- H. Structural effects of iron oxide nanoparticles and iron ions on the hydrothermal carbonization of starch and rice carbohydrates. Small 2006;6(2):756–9.
[30] Vigneshwaran N, Kumar S, Kathe AA, Varadarajan PV, Prasad V. Functional finishing of cotton fabrics using zinc oxide-soluble starch nanocomposites. Nanotechnology 2006;17:5087–95.
[31] Chowdhury PS, Arya PR, Raha K. Green synthesis of nanoscopic iron oxide particles: a potential oxidizer in nanoenergetics. Synthesis and Reactivity in Inorganic, Metal-Organic, and Nano-Metal Chemistry 2007;37:447–51.
[32] Nidhin M, Indumathy R, Sreeram KJ, Nair BU. Synthesis of iron oxide nanoparticles of narrow size distribution on polysaccharide templates. Bulletin of Materials Science 2008;31(1):93–6.
[33] Mumalo-Djokic D, Stern WB, Taubert A. Zinc oxide/carbohydrate hybrid materials via mineralization of starch and cellulose in the strongly hydrated ionic liquid tetrabutylammonium hydroxide. Crystal Growth and Design 2008;8(1):330–5.
[34] Nakamoto K. Infrared and Raman spectra of inorganic and coordination compounds. New York: Wiley; 1986.
[35] Siegel GA, Bartlet RA, Decker D, Olmstead MM, Power PP. Charge delocalization in ruthenium-quinone complexes. Structural characterization of bis (bipyridine)(3,5-di-tert-butylsemiquinonato)ruthenium(II) perchlorate and trans-bis(4-tert-butylpyridine)bis(3,5-di-tert-butylquinone)ruthenium. Inorganic Chemistry 1987;26:1769–73.
[36] Adams RW, Martin RL, Winter G. Possible ligand field effects in metal-oxygen vibrations of some first-row transition metal alkoxide. Australian Journal of Chemistry 1967;20(4):773–4.
[37] Kruger A, Winter G. Magnetism, electronic spectra, and structure of transition metal alkoxides. VIII. Nickel halo methoxides. Australian Journal of Chemistry 1970;23(1):1–14.
[38] Barraclough CG, Bradley DC, Lewis J, Thomas IM. The infrared spectra of some metal alkoxides, trialkylsilyloxides, and related silanols. Journal of Chemical Society; 1961:2601–5.
[39] Pacewska B, Keskr M. Thermal transformations of aluminium nitrate hydrate. Thermochimica Acta 2002;385:73–80.
[40] Gyoryová K, Balek V. Thermal stability of new zinc acetate-based complex. Journal of Thermal Analysis and Calorimetry 1993;40:519–32.
[41] Zayat M, Levy D. Blue $CoAl_2O_4$ particles prepared by the sol-gel and citrate-gel methods. Chemistry of Materials 2000;12:2763–9.
[42] Štangar UL, Orel B, Krajnc M, Korošec RC, Bukovec P. Sol-gel-derived thin ceramic $CoAl_2O_4$ coatings for optical applications. Materiali in Tehnologije 2002;36:387–93.
[43] Štangar UL, Orel B, Krajnc MJ. Preparation and spectroscopic characterization of blue $CoAl_2O_4$ coatings. Journal of Sol-Gel Science and Technology 2003;26:771–5.
[44] Lever ABP. Inorganic electronic spectroscopy. Amsterdam: Elsevier; 1984.
[45] Radovanovic PV, Gamelin DRJ. Electronic absorption spectroscopy of cobalt ions in diluted magnetic semiconductor quantum dots: demonstration of an isocrystalline core/shell synthetic method. Journal of the American Chemical Society 2001;123:12207–14.
[46] El Habra N, Crociani L, Sada C, Zanella P, Casarin M, Rossetto G, et al. MOCVD of $CoAl_2O_4$ thin films from $\{Co[Al(O\ ^iC_3H_7)_4]_2\}$ as precursor. Chemistry of Materials 2007;12:3381–6.
[47] Zayat M, Levy D. Blue $CoAl_2O_4$ particles prepared by the sol–gel and citrate–gel methods. Chemistry of Materials 2000;12:2763–9.
[48] Barreca D, Massignan S, Daolio S, Fabrizio M, Piccirillo C, Armelao L, et al. Composition and microstructure of cobalt oxide thin films obtained from a novel cobalt(II) precursor by chemical vapor deposition. Chemistry of Materials 2001;13:588–93.